

# UNCORRECTED PROOFS

## Recent Macaronesian kinematics from GNSS ground displacement analysis

IGNACIO BARBERO<sup>1,7</sup>, CRISTINA TORRECILLAS<sup>2</sup>, RAÚL PÁEZ<sup>3</sup>, GONÇALO PRATES<sup>4,5,6</sup>  
AND MANUEL BERROCOSO<sup>4</sup>

- 1      Escuela Técnica Superior de Ingeniería, Universidad de Sevilla, Sevilla, Spain  
(ignacio\_barbero@us.es)
- 2      Departamento de Ingeniería Gráfica, Escuela Técnica Superior de Ingeniería, Universidad de  
Sevilla, Spain (torrecillas@us.es)
- 3      Departamento de Estadística e Investigación Operativa, Facultad de Ciencias, Universidad de  
Cádiz, Spain (raul.paez@uca.es)
- 4      Laboratorio de Astronomía, Geodesia y Cartografía. Universidad de Cádiz, Puerto Real,  
Cádiz, Spain (manuel.berrocoso@uca.es)
- 5      Centro de Estudos Geográficos, IGOT, Universidade de Lisboa, Lisboa, Portugal
- 6      Instituto Superior de Engenharia, Universidade do Algarve, Faro, Portugal (gprates@ualg.pt)
- 7      Ministerio de Hacienda, Dirección General del Catastro, Spain<sup>1</sup>

Received: March 21, 2020; Revised: August 24, 2020; Accepted: November 5, 2020

### ABSTRACT

Macaronesia is a complex oceanic region spanning three tectonic plates in the north-east Atlantic ocean. It is composed of four archipelagos, widely distributed and limited to the east by the Iberian Peninsula and north-western coast of Africa. This study aims to clarify recent Macaronesian kinematics from 19 GNSS stations located on the four archipelagos and the Iberian and African coastlines. The analysis is based on nearly 15 years of common data acquisition and aimed to detect new effects of intraplate tectonics or similar local/regional events consistent with calculated ground displacements. Evaluating the GNSS stations residual velocities relative to those expected from the NNR-MORVEL56 model, higher residuals were found at continental coastal stations (Africa) than at oceanic ones (Canaries and Madeira). From the computed strain rate map, the possible existence of a shear zone connecting the Gloria and Transmoroccan fault systems, already mentioned by other authors, was depicted. Cluster statistical analysis of the horizontal residual velocities helped to identify tectonic boundaries in Macaronesia and four groups of analogous intraplate residual velocities within this region. Three of four groups were identified in the Azores, highlighting the African-Nubian-Eurasian diffuse plate boundary in this region. Furthermore, in the Canary Islands, two distinct kinematic behaviours were detected, possibly due to the activity along a previously detected tectonic fault between Tenerife and Gran Canaria, where some stations have similar intraplate residuals to those at Madeira and Cape Verde stations, while others have similar intraplate residuals to those of continental stations. Finally, all stations on

1 oceanic crust, except Cape Verde, present recent ground subsidence which may be  
 2 attributed to isostatic adjustment.  
 3

4 Keywords: continuous GNSS time series, Canary Islands, cluster analysis, strain  
 5 rate analysis, isostatic adjustment

## 6 1. INTRODUCTION

7 Macaronesia is the collective name given to the group of islands that lie in the north-  
 8 east Atlantic ocean between 10°N and 40°N latitude (Fig. 1). These islands form four  
 9 archipelagos, which are, from north to south: the Azores, Madeira, the Canary Islands and  
 10 Cape Verde. The Mid-Atlantic Ridge (MAR) marks its western boundary and the Gloria  
 11 transform fault its northern boundary (Scheidegger, 2002). However, the Azores lie on  
 12 a triple junction, where the North American, Eurasian and Nubian Plates interact.  
 13 Although these archipelagos are widely distributed, these islands and the coastlines of  
 14 north-west Africa and the Iberian Peninsula are the available emerged land where Global  
 15 Navigation Satellite System (GNSS) observations can be made.

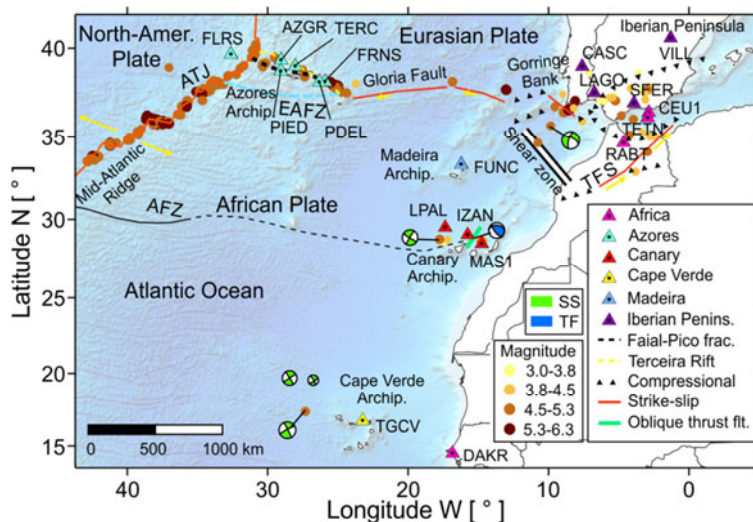


**Fig. 1.** Macaronesian GNSS stations and African-Nubian plate boundary elements. Focal mechanisms from the ISC catalogue, within each event from the ISC Bulletin for focal mechanism solutions from the *International Seismological Centre (2019)*; between 40°W–0°W and 15°N–40°N and weighted by the earthquake magnitude. A seismic hypocentre depth limit < 70 km and a magnitude  $M_w > 3.0$  were established between 2000/01/01 and 2016/12/31. Standard regime of normal faulting (NF), thrust faulting (TF), strike-slip (SS) and unknown (U) is shown; ETOPO1 basemap is obtained from NOAA National Centres for Environmental Information (NCEI). Map is represented in Mercator projection over WGS84 Earth reference system. AFZ: Atlantis Fracture Zone, EAFZ: East Azores Fracture Zone, ATJ: Azores Triple Junction, TFS: Transmoranocan Fault System. See Table 1 for GNSS station codes.<sup>2</sup>

**Table 1.** Continuous GNSS stations used with public access data and managed by public institutions: International GNSS Service (IGS, <http://www.igs.org>), EUREF Permanent GNSS Network (EPN, <http://www.epnch.oma.be>), Rede Nacional de Estações Permanentes GNSS (ReNEP, <https://renep.dgterritorio.gov.pt/estacoes>).

GNSS	Location	Region	Owner	Start [year, day#]	End [year, day#] <sup>3</sup>
FLRS	Flores	Azores	IGS	2008,159	2015,090
PDEL	São Miguel	Azores	IGS	2000,241	2015,090
TERC	Terceira	Azores	EPN	2008,016	2015,090
PIED	Pico	Azores	ReNEP	2008,016	2012,177
FRNS	São Miguel	Azores	ReNEP	2008,016	2014,005
AZGR	Graciosa	Azores	ReNEP	2009,347	2012,177
FUNC	Madeira	Madeira	IGS	2005,314	2015,090
MAS1	Gran Canaria	Canary Islands	IGS	2000,211	2015,090
IZAN	Tenerife	Canary Islands	EPN	2008,110	2015,090
LPAL	La Palma	Canary Islands	EPN	2001,179	2015,090
TGCV	Sal	Cape Verde	IGS	2000,004	2014,155
CASC	Portugal	Iberian Peninsula	EPN	2000,241	2015,090
LAGO	Portugal	Iberian Peninsula	EPN	2000,229	2015,090
SFER	Spain	Iberian Peninsula	EPN	2000,242	2015,090
VILL	Spain	Iberian Peninsula	IGS	2000,116	2015,090
CEU1	Spain	Africa	EPN	2008,314	2015,090
TETN	Morocco	Africa	EPN	2002,083	2015,090
RABT	Morocco	Africa	EPN	2000,166	2015,090
DAKR	Morocco	Africa	IGS	2012,209	2015,090

Only a few studies have focused on Macaronesian kinematics, since rigidity, continuity and insignificant seismicity seem to be fundamental aspects of the main plate, the African-Nubian, regardless of the activity of both the MAR and Nubian-Eurasian plate boundaries (Fig. 2). Additionally, its low speed relative to its neighbouring plates of nearly 1 mm yr<sup>-1</sup> (*Burke and Wilson, 1972; Kogan et al., 2000; Malservisi et al., 2013*) and its minimum internal strain, with no significant deformation with values <1 mm yr<sup>-1</sup> (*Calais et al., 2003; McClusky et al., 2003; Serpelloni et al., 2007*), are other suitable descriptions for this plate. The global stress map database (*Heidbach et al., 2018*) and some physical models of Macaronesia (*Geyer et al., 2016; Jiménez-Munt and Negredo, 2003*) are other sources where low values of internal stress are shown.

Observations from continuous GNSS stations in Macaronesia started in 2000 with a limited number of permanent stations. Most previous studies were carried out by mixing observations from periodic or episodic GNSS campaigns in their calculations (*Barbero et al., 2018; Garcia et al., 2014; Marques et al., 2013a, 2015; Mendes et al., 2013; Pérez-Peña et al., 2010; Prates et al., 2013; Vernant et al., 2010*). Overall, these locally or regionally determined velocities are similar to the velocities of geologic plate motion computed from global models such as NNR-MORVEL56 (*DeMets et al., 2010*) and NNR-NUVEL1A (*DeMets et al., 1994*), and azimuths only disagreeing slightly by a few degrees.

In 2004, the unusual increase in seismic events in Tenerife, with some earthquakes felt by the population, and the underwater eruption off the coast of El Hierro augmented volcanic studies in the Canary Islands (*Dominguez-Cerdeña et al., 2011; Garcia et al., 2014; Prates et al., 2013*). One of these recent studies focused on Tenerife showed distinct kinematics between this island and the neighbouring island of Gran Canaria, with different horizontal velocities computed over 10 years (*Barbero et al., 2018*). The increase of permanent GNSS stations in Macaronesia and their data accessibility since 2000 offer the possibility of carrying out a precise ground displacement analysis of the whole Canary archipelago and the opportunity of finding similarities and differences to the kinematics of other archipelagos. Therefore, the purpose of this study is to evaluate the regional geodynamics of the Canary Islands and provide an overall interpretation of the recent intraplate kinematics of the African-Nubian Plate. For this, velocities between May 2000 and March 2015 were calculated for 19 stations, aiming at accuracy of less than  $1 \text{ mm yr}^{-1}$  over such long periods (*Blewitt and Lavallée, 2002; Bos et al., 2010*). Furthermore, a statistical cluster analysis was performed to identify and group residuals with similar velocity and, finally, strain maps were generated to define intraplate kinematics in Macaronesia and, particularly, in the Canary Islands.

## 2. REGIONAL SETTING

Although all archipelagos in Macaronesia have a minimum of five islands and volcanic origin, the nature of this volcanism is not always clear (*Geldmacher et al., 2006;*

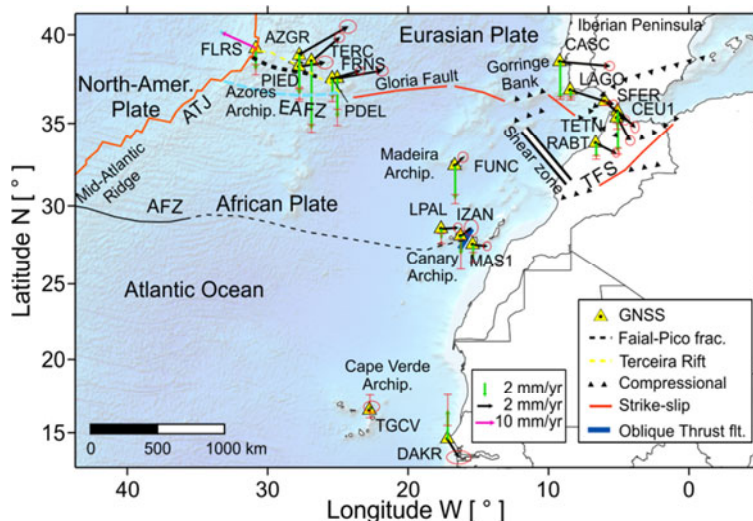


**Fig. 2.** Macaronesia residual kinematic map for 2000–2015. The arrows represent residual horizontal and vertical velocities at GNSS stations after removing NNR-MORVEL56. Biases with a 95% confidence level are shown as ellipses for the horizontal and intervals for the vertical velocities. AFZ: Atlantis Fracture Zone, EAFZ: East Azores Fracture Zone, GB: , TFS: Transmoroccan Fault System.<sup>4</sup> See Table 1 for station codes.<sup>5</sup>

1 *Métrich et al., 2014; Pacheco et al., 2013; Ramalho, 2011*). The ages of their old  
2 seamounts date from 142 Myr to 200000 years (*von den Bogaard, 2013*). From the north-  
3 west, near the MAR, the first of the four archipelagos is the Azores which includes nine  
4 islands aligned NW-SW (see Fig. 1). The two most westerly islands, Flores and Corvo,  
5 are located on the North American plate. The other seven islands lie to the east of the  
6 MAR, arranged in two groups: the central group includes Graciosa, Terceira, São Jorge,  
7 Faial and Pico, while the eastern group includes São Miguel and Santa Maria. Both groups  
8 are in the vicinity of the Eurasian-African-Nubian plate boundary. This region shows an  
9 anomalously thick crust (*Silveira et al., 2010*) with modern volcanism (1957 Capelinhos  
10 volcano in Faial and 1999–2000 underwater eruption near Terceira) (*Pacheco et al., 2013*)  
11 and recent moderate to high magnitude seismicity (1980 -  $M7.2$ , 1997 -  $M5.1$  and 1998 -  
12  $M6.2$  earthquakes) (*Borges et al., 2007*). The most important geological structures are the  
13 Terceira Rift, aligned by Graciosa, Terceira and São Miguel islands, and the East Azores  
14 Fracture Zone (EAFZ).

15 The archipelagos of Madeira, the Canary Islands and Cape Verde are concentrated in  
16 the east Atlantic Ocean away from plate boundaries. The Madeira archipelago comprises  
17 Madeira, Porto Santo, Deserta Grande and Selvagem Grande islands. The most recent  
18 volcanic eruptions occurred 6500 years ago. The Canary Islands archipelago is formed by  
19 seven major islands: La Palma, El Hierro, La Gomera, Tenerife, Gran Canaria,  
20 Fuerteventura and Lanzarote, located less than 100 km off the north-west coast of Africa.  
21 In the past 500 years, volcanic eruptions have been recorded and documented at El Hierro,  
22 Lanzarote, Tenerife and La Palma. The Cape Verde archipelago lies 450–600 km off the  
23 western coast of Africa and is composed of ten islands: Santo Antão, São Vicente, Santa  
24 Luzia, São Nicolau, Sal, Boa Vista, Maio, Santiago, Fogo and Brava, arrayed in a west-  
25 facing horseshoe shape. The volcanic activity probably started in the Oligocene/Miocene  
26 and extended well into the Holocene. Historical eruptions are unknown except on Fogo,  
27 a highly active volcano whose last eruptions occurred in 1995 and 2014 (*Ramalho, 2011*).

### 28 3. RECENT NUBIAN KINEMATICS

29 The African plate consists of two subplates separated by the East African rift system:  
30 the Nubian to the west and Somalian to the east. Most of Macaronesia is part of the  
31 African-Nubian Plate. The main Atlantic fractures present in this area are related to  
32 different velocities of the MAR opening revealed by two main transform faults: the Gloria  
33 Fault, linked to the MAR by the EAFZ and the Terceira Rift (*Fernandes et al., 2006*), and  
34 the Atlantis Fracture Zone (AFZ), extending from the MAR to the Transmoroccan Fault  
35 System (TFS) and limiting the Morocco subplate (*Mantovani et al., 2007*) (Fig. 1). The  
36 Gloria transform fault, which is part of the Nubian-Eurasian plate boundary, involves  
37 predominantly right-lateral compression along the eastern segment, strike-slip along the  
38 central segment and oblique extension on the westernmost segment in the Azores.  
39 *Mantovani et al. (2007)* proposed another shear zone connecting the Gloria Fault and the  
40 EAFZ propagation towards the TFS, marking the Atlantic-Mediterranean transition,  
41 where the Nubian-Eurasian plate boundary changes to a diffuse transpressive region,  
42 comprising a wide range of active deformation. Other authors have suggested that  
43 a subduction zone is forming at the south-west of the Iberian Peninsula, as a result of both

1 propagations of the Gibraltar Arc compressive stresses and pressures related to the large-  
2 scale Nubian-Eurasian convergence (*Duarte et al., 2013*).

3 Mostly, GNSS calculations in the African-Nubian Plate offer values with slight  
4 velocity differences relative to global models, around  $\pm 1 \text{ mm yr}^{-1}$ , but nevertheless show  
5 greater differences in azimuth. Specifically, from campaign and continuous GNSS data  
6 from 2001 until 2013, the African-Nubian Plate was inferred to move  $4.6 \pm 0.3 \text{ mm yr}^{-1}$   
7 toward S87.9°W (167.9°)  $\pm 3.3^\circ$  (95% uncertainty) relative to Eurasia in the Azores  
8 (*Marques et al., 2013a*), similar to the NNR-MORVEL56 model value of  
9  $4.5 \pm 0.4 \text{ mm yr}^{-1}$  toward S68.1°W (148.1°)  $\pm 2.8^\circ$  (*DeMets et al., 2010*), mainly  
10 depicting an azimuth difference of nearly  $20^\circ$ . Another relevant aspect is that the NNR-  
11 NUVEL1A model (*DeMets et al., 1994*) considers Terceira (station TERC, see Fig. 1),  
12 Graciosa (station AZGR) and eastern São Miguel (station FRNS) as part of the Eurasian  
13 Plate, and western São Miguel (station PDEL) and Pico (station PIED) as part of the  
14 African-Nubian Plate. The horizontal velocity of the African-Nubian Plate computed by  
15 the UNAVCO plate motion calculator (<https://www.unavco.org/software/geodetic-utilities/plate-motion-calculator/plate-motion-calculator.html>), with Eurasia as the  
16 reference plate, was  $4.0\text{--}4.2 \text{ mm yr}^{-1}$  with an azimuth of S65°–75°W (245°–255°) for  
17 both stations (PDEL and PIED). Within the central group, the Pico/Faial volcanic ridge  
18 was shown to move mostly with the African-Nubian Plate, Terceira island moves mostly  
19 with the Eurasia Plate, and São Jorge island has an intermediate position between African-  
20 Nubian and Eurasian Plates (*Marques et al., 2013a; Mendes et al., 2013*). Similar values  
21 were calculated by *Borges et al. (2007)* who found an average seismic strain rate of about  
22  $4.4 \text{ mm yr}^{-1}$  with a NW direction for the period 1980–1998. Subsidence was detected on  
23 Terceira island between 1999 and 2006 based on GPS (*Miranda et al., 2012*) and also  
24 between 2001 and 2013 by combining InSAR and GPS techniques (*Marques et al., 2015*).  
25

26 Near Gibraltar, velocities in stations TENT, SFER and CEU1 present values between  
27  $4.4$  and  $4.7 \text{ mm yr}^{-1}$  and azimuths of N40°–50°W (310°–320°) from NUVEL1A, with  
28 Eurasia as the reference plate, using the UNAVCO Plate Motion Calculator, while  
29 southwards horizontal velocity magnitude decreases to  $3.9 \text{ mm yr}^{-1}$  and an azimuth of  
30 N41°W (319°) in station RABT. *Koulali et al. (2011)* inferred a south-westward motion of  
31 the Rif Mountains in northern Morocco<sup>6</sup>, with velocities between  $3.5$  and  $4 \text{ mm yr}^{-1}$ .  
32 *McClusky et al. (2003)* determined an NW-SE convergence within the Mediterranean,  
33 with a larger westerly component of motion than NUVEL1A, with Eurasia as the  
34 reference plate, ranging from  $5.4 \pm 1 \text{ mm yr}^{-1}$  in the Eastern Mediterranean to  
35  $4.5 \pm 1 \text{ mm yr}^{-1}$  near Gibraltar. The study of *Pérez-Peña et al. (2010)* found slight  
36 differences in azimuth between their calculations and NUVEL1A between 1995 and 2005  
37 in Southern Spain. Finally, *Vernant et al. (2010)* showed that the deformation associated  
38 with the Nubian-Eurasian plate boundary that occurs in the Betic-Rif-Alboran domain has  
39 velocities of around  $4 \text{ mm yr}^{-1}$ , and showed azimuths in clockwise rotation between  
40 CASC and RABT stations between 1997 and 2009.

41 In the region defined by Madeira, the Canary Islands and Cape Verde archipelagos,  
42 horizontal velocities follow the MAR transform fault direction of SW-NE. A recent GPS  
43 study from 1998–2005 showed similar velocities between MAS1 and the continental  
44 TETN station and slight differences in azimuth between both and the TGCV station

1 (*Serpelloni et al., 2007*). *Martín et al. (2014)* showed similar horizontal velocities in all  
 2 Canary Islands, between 2002 and 2009, so no strain within the archipelago was detected  
 3 with root mean square (RMS) values of 2 mm. However, the Canary Islands have  
 4 experienced an increase in seismic activity since 2003, which is considered a precursor of  
 5 the recent volcanic unrest and eruption on El Hierro island (*López et al., 2017*) and an  
 6 overall uplift until 2011 and subsidence from then on has also been detected (*López et al.,*  
 7 *2017*). Finally, in Cape Verde, overall subsidence has been detected with data from  
 8 Sentinel-1 between 2017 and 2018 (*Dias et al., 2018*).

#### 9           4. GNSS DATA

10         In order to study the kinematics of Macaronesia, a total of 19 continuous GNSS  
 11 stations were selected, managed by public institutions and with public data access; six  
 12 GNSS stations were selected in the Azores (AZGR, PIED, TERC, PDEL, FRNS and  
 13 FLRS), one in Madeira (FUNC), one in Cape Verde (TGCV), three in the Canary Islands  
 14 (IZAN, LPAL and MAS1), four on the Iberian Peninsula (VILL, SFER, LAGO and  
 15 CASC) and four on the African western coastline (TENT, CEU1, RABT and DAKR)  
 16 (Table 1 and Fig. 1). The observation window span was nearly 15 years, from May 2000  
 17 to March 2015. The most representative continuous GNSS stations were selected based on  
 18 their long and stable time series.

#### 19           5. METHODOLOGY AND RESULTS

##### 20           5.1. GNSS data processing

21         The GNSS data were processed using Bernese software v.5.0, particularly the Bernese  
 22 Processing Engine module (*Dach et al., 2011*), with satellite antenna bias corrections and  
 23 REPRO2 files (daily orbits, satellite clocks and Earth rotation parameters) (*Rebischung et*  
 24 *al., 2016*). A sampling rate of 30 s and a 10° elevation mask were applied. Hourly  
 25 tropospheric refraction corrections to the combined *Saastamoinen (2013)* and *Niell (2004)*  
 26 models were computed. The average distance between stations was 1562 km, the shortest  
 27 distance being 483 km and the longest 3105 km, so the Quasi Ionosphere-Free algorithm,  
 28 recommended for long baselines, was applied to resolve ambiguity (*Mervart, 1995*). Also,  
 29 the Ocean Tide Load bias was corrected by the GOT00.2 model (*Ray, 1999; Scherneck*  
 30 *and Bos, 2002*).

31         The VILL station, located on the Iberian Peninsula on the Eurasia Plate, was selected  
 32 as the reference in the differential positioning ionosphere-free mode, due to its very stable  
 33 time series in this time span (<http://www.igs.org/network>). The known reference station  
 34 position and velocity and precise satellite ephemeris data allow the daily coordinates to be  
 35 computed for each station in the ITRF2008 reference frame. From daily topocentric  
 36 positions (east, north and up), time series velocities were computed. The model fitted to  
 37 these time series was:

$$38 \quad x(t) = x_0 + v_x(t - t_0) + \sum_{i=1}^2 (a_i \sin(\omega_i(t - t_0)) + b_i \cos(\omega_i(t - t_0))) + \varepsilon(t), \quad (1)$$

1 where  $x(t)$  is the value of the topocentric coordinate at time  $t$ ,  $t_0$  is the reference epoch,  
 2  $x_0$  is the initial position,  $v_x$  is the velocity,  $\omega_i$  is the angular frequency for harmonic  
 3 components, and  $a_i$  and  $b_i$  are the amplitudes of the sine and cosine, respectively. Finally,  
 4  $\varepsilon(t)$  represents the noise.

5 HECTOR software was applied to estimate velocities, as well as other parameters and  
 6 the noise model (Bos et al., 2013). This software uses maximum likelihood estimation  
 7 (MLE) to estimate these parameters and related uncertainties. White noise and power-law  
 8 noise close to flicker noise with a spectral index of  $-1$  were considered as the optimum  
 9 noise models to describe the stochastic part of the time series (He et al., 2017; Klos et al.,  
 10 2018, 2019; Williams et al., 2004).

11 The horizontal velocities contain the tectonic plate motion normally defined by  
 12 rotation around a Euler pole. NNR-MORVEL56 (Argus et al., 2011) defines the African-  
 13 Nubian Plate Euler pole at  $47.68^\circ\text{N}$  and  $68.44^\circ\text{W}$  with an angular velocity of  
 14  $0.292^\circ \text{ Ma}^{-1}$ . The horizontal velocities calculated by this model were subtracted from the  
 15 ITRF2008 horizontal velocities of each GNSS station using EPC software (Goudarzi et  
 16 al., 2014). Therefore, the eastward and westward<sup>8</sup> horizontal residual velocities of the  
 17 African-Nubian Plate motion ( $dV_{E\text{ Eul}}$  and  $dV_{N\text{ Eul}}$  respectively) and module ( $dV_{Eul}$ )<sup>9</sup> for  
 18 each GNSS station were computed (see Fig. 2 and Table 2).

19 Analysing the horizontal residual velocities, without taking into account station FLRS  
 20 located on the North American Plate, some aspects can be highlighted:

- 21 • All GNSS stations in the Azores archipelago have similar magnitudes and  
 22 azimuths with directions between E and NE.
- 23 • There is continuous azimuth rotation of stations on the Iberian Peninsula and  
 24 Gibraltar, depicted by the horizontal residual velocities in CASC, LAGO, SFER,  
 25 CEU1 and TETN. These stations show similar magnitudes to those from Azores  
 26 stations, although those not on the African-Nubian Plate present, as expected,  
 27 higher-velocity residuals.
- 28 • All stations on the Canary Islands have small horizontal velocity residuals with E  
 29 to NE azimuths, as does FUNC in the Madeira archipelago.
- 30 • DAKR and RABT, on the African western coastline, have SE azimuths and higher  
 31 magnitudes than the Canary Islands.
- 32 • TGCV in Cape Verde presents no horizontal velocity residual above the GNSS  
 33 accuracy, hence agreeing with NNR-MORVEL56 model velocity for the African-  
 34 Nubian Plate there.
- 35 • Finally, overall subsidence was detected in all Macaronesian stations, except for  
 36 DAKR and TGCV, with higher values north of São Jorge Island in the Azores  
 37 (TERC nearly  $-9 \text{ mm yr}^{-1}$  and AZGR with  $-5 \text{ mm yr}^{-1}$ ).

**Table 2.** Geographical coordinates, first and final date of data<sup>10</sup>, easting ( $V_E$ ), northing ( $V_N$ ) and vertical ( $V_U$ ) velocities, all with respect to the ITRF2008 reference frame with uncertainties and the corresponding residuals after correction from the NNR-MORVEL56 Nubian Euler pole ( $dV_{E\_Eul}$ ,  $dV_{N\_Eul}$  and module  $dV_{Eul}$ ) for each GNSS station. Except for coordinates, all the values in mm yr<sup>-1</sup>.<sup>11</sup>

GNSS	Lat. N [°]	Lon. E [°]	$V_E$	$V_N$	$V_U$	$\sigma_E$	$\sigma_N$	$\sigma_U^{12}$	$dV_{N\_Eul}$	$dV_{E\_Eul}$	$dV_{Eul}$
AZGR	39.08786	-28.02295	14.52	17.87	-5.20	1.21	0.74	1.85	3.68	6.42	7.40
CASC	38.69342	-9.41852	18.25	18.14	-4.74	0.37	0.38	0.39	-0.56	6.55	6.57
CEU1	35.89197	-5.30639	15.96	17.41	-5.32	0.29	0.53	0.81	-2.09	2.27	3.09
DAKR	14.72090	-17.43950	21.15	14.68	3.87	2.56	0.76	4.07	-2.32	1.45	2.74
FLRS	39.45383	-31.12639	-10.59	21.43	-2.84	0.64	0.45	1.32	8.13	-18.10	19.84
FRNS	37.76933	-25.30821	15.11	16.02	-5.12	0.63	0.49	2.15	1.02	5.92	6.01
FUNC	32.64795	-16.90762	13.93	18.23	-4.41	0.43	0.46	1.18	1.13	1.04	1.54
IZAN	28.30806	-16.49968	18.16	17.06	-2.40	0.30	0.31	0.39	1.12	1.36	1.76
LAGO	37.09894	-8.66838	16.58	17.06	-1.05	0.32	0.40	1.36	-1.83	5.67	5.96
LPAL	28.76387	-17.89383	16.94	17.21	-1.25	0.26	0.34	1.32	0.16	2.19	2.20
MAS1	27.76374	-15.63328	12.87	15.95	-1.68	0.33	0.27	0.81	-0.18	1.85	1.86
PDEL	37.74775	-25.66277	11.89	14.77	-2.59	1.13	0.67	1.36	1.06	3.68	3.83
PIED	38.41382	-28.03246	16.73	17.85	-3.54	0.19	0.26	0.46	0.57	3.40	3.45
RABT	33.99810	-6.85429	15.93	16.94	-1.87	0.33	0.37	0.52	-1.35	2.64	2.97
SFER	36.46435	-6.20564	12.21	17.50	-0.24	0.41	0.39	1.04	-2.45	2.63	3.59
TERC	38.71899	-27.15299	15.53	16.31	-8.81	0.36	0.39	0.80	3.11	3.72	4.85
TETN	35.56160	-5.36300	18.82	16.00	-1.18	1.10	0.53	3.00	-3.18	1.73	3.62
TGCV	16.75477	-22.98276	19.23	16.32	0.47	0.21	0.23	0.05	0.40	0.23	0.46
VILL	40.44359	-3.95198	14.52	17.87	-1.75	1.21	0.74	1.85	-3.38	7.04	7.81
Average (without FLRS)			16.22	16.87							

## 1                   5.2. Cluster analysis

2                   Statistical cluster analysis (*Kaufman and Rousseeuw, 1990*) was performed to evaluate  
 3                   similarities in the horizontal residual velocities and thus to group stations based on their  
 4                   kinematics. This method has been previously applied to GNSS data in California to  
 5                   classify stations within the San Andres fault system (*Savage and Simpson, 2013; Simpson  
        et al., 2012*) and is widespread in GNSS studies (*Özdemir and Karşioğlu, 2019*).

7                   The  $k$ -means clustering method (*Larose and Larose, 2014*) was applied to the  
 8                   horizontal residual velocity space. This approach groups the data set into a defined  
 9                   number of clusters,  $k$ . The algorithm consists of randomly assigned  $k$  records (residual  
 10                  velocities) as the initial cluster centre locations. For each record, the nearest cluster centre  
 11                  using the Euclidean distance was found. A subset of the records was assigned to each  
 12                  centroid, representing partition of the data set or cluster. For each of the  $k$  clusters, the  
 13                  mean value of the records was found, named the centroid, and the location of each cluster  
 14                  centre updated to the new value of the centroid. This process was repeated until the  
 15                  centroids no longer changed or there was no significant shrinkage in the mean squared

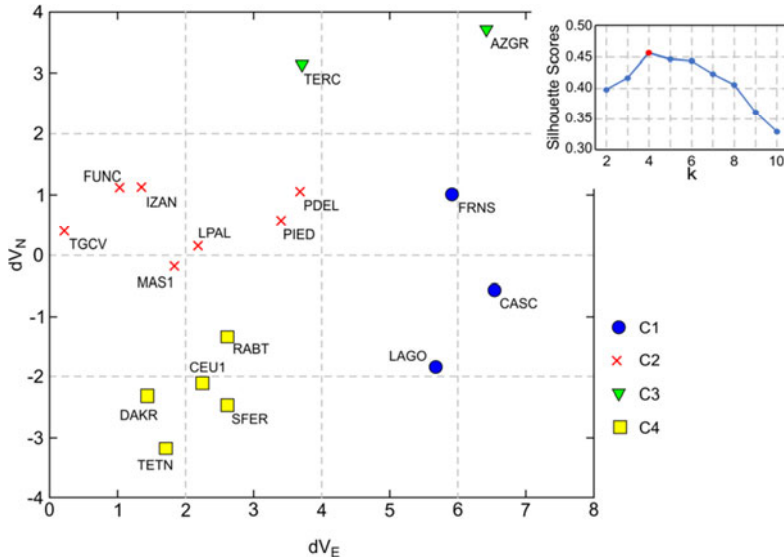


**Fig. 3.** Four clusters obtained from the cluster analysis using residual north and east velocity components ( $dV_N$  and  $dV_E$ ) in the studied period. Inset shows the mean silhouette values of data grouped from two to ten clusters; mean value is maximum for number of clusters  $k = 4$ . See Table 1 for GNSS station codes.<sup>13</sup>

1 error. To determine the optimal number of clusters  $k$ , the silhouette criterion (Rousseeuw,  
 2 1987) was chosen; see the top inset of Fig. 3. The stations VILL and FLRS were excluded  
 3 from this process because VILL was chosen as a reference station and FLRS is a cluster  
 4 itself due to its very different velocity compared to the other stations, as it is the only one  
 5 on the North American Plate. The silhouette criterion suggested that the optimal number  
 6 of clusters  $k$  was 4 (Fig. 3). Other clustering criteria such as hierarchical complete and  
 7 ward or agglomerative nesting determined the same number. The clustering detected  
 8 Eurasian (C1: LAGO, CASC and FRNS), Nubian-Macaronesian Islands (C2: PIED,  
 9 PDEL, FUNC, LPAL, IZAN, MAS1 and TGCV), Terceira Rift (C3: AZGR and TERC)  
 10 and Gibraltar-African (C4: SFER, CEU1, TETN, RABT and DAKR) behaviours.  
 11 Grouping of the Azores stations in three different clusters (C1, C2 and C3) highlights the  
 12 tectonic complexity within this archipelago and, further, subdivision into five and six  
 13 clusters affected only the Azores stations (AZGR, TERC, PDEL and PIED). Table 3  
 14 shows the mean horizontal residual velocities and the mean azimuths for each group.

### 15 5.3. Strain rate computation

16 A first approximation to the velocity field description may be given by the  $t$  parameter  
 17 as defined by Teza et al. (2012). This parameter highlights differences in sign and  
 18 magnitude between the easting ( $V_E$ ) and northing ( $V_N$ ) components of the horizontal  
 19 velocity residuals and, hence, identifies regions with similar kinematic behaviours and  
 20 their corresponding boundaries. The  $t$  parameter is given as:

**Table 3.** Kinematic clusters with mean horizontal residual velocity ( $V$ ), mean azimuth ( $Az$ ) and corresponding root mean square errors ( $\sigma$ ) in ITRF2008 reference frame.<sup>14</sup>

	$V$ [mm yr <sup>-1</sup> ]	$\sigma_V$ [mm yr <sup>-1</sup> ]	$Az$ [°]	$\sigma_{Az}$ [°]
Eurasian Nubian-Macaronesian Islands Terceira Rift Gibraltar-African	6.2	0.3	101.4	9.2
	2.2	1.2	65.5	24.6
	6.1	1.8	55.1	7.1
	3.2	0.4	316.4	13.8

$$t = \frac{V_E - V_N}{V_E + V_N}. \quad (2)$$

As defined, if velocity components present the same sign, they have values in the interval  $[0, 1]$  for  $|V_E| > |V_N|$  and in the interval  $[-1, 0]$  for  $|V_E| < |V_N|$ , whereas if velocity components present opposite signs, they have values in the intervals  $[1, \infty]$  and  $[-\infty, 1]$  for  $|V_E| > |V_N|$  and  $|V_E| < |V_N|$ , respectively. The  $t$  values were also computed in the nodes of a regular grid of  $300 \times 300$  km, without nodes inside a buffer of 300 km from each station. In these regular grid nodes, horizontal velocities were computed in ITRF2008 with the UNAVCO Plate Motion Calculator, with values of  $16.3$  mm yr<sup>-1</sup> for easting and  $17.1$  mm yr<sup>-1</sup> for northing ( $23.6$  mm yr<sup>-1</sup> in magnitude), which are similar to the mean horizontal velocity for all GNSS stations in this study, with values of  $16.2 \pm 0.5$  mm yr<sup>-1</sup> for easting and  $16.8 \pm 0.6$  mm yr<sup>-1</sup> for northing ( $23.4 \pm 0.8$  mm yr<sup>-1</sup> in magnitude). Finally, the ordinary kriging technique was applied to interpolate the  $t$  parameter from this regular grid and GNSS station horizontal velocity. The  $t$  prediction standard error rates were calculated to show the interpolation quality rates (Fig. 4a).

Following Fig. 4a, the  $t$  parameter distinguishes four regions in Macaronesia and allows a deeper analysis:

- The Azores central and eastern islands region which, from east to west, presents positive to negative  $t$  values where two major structures are identified: the Terceira Rift and Pico-Faial volcanic ridge (Marques *et al.*, 2013b; Silva *et al.*, 2018).
- The Gibraltar arc region with low positive  $t$ -values to the east and near zero to the west.
- The Madeira and Canary Islands regions have similar negative  $t$  values, though these values are lower in the islands of Madeira, Tenerife, Gomera, La Palma and El Hierro compared to Gran Canaria, Lanzarote and Fuerteventura, possibly due to an alignment of high seismic activity between the islands of Tenerife and Gran Canaria (Fig. 2).
- Finally, the Cape Verde and Dakar regions with positive  $t$  values, near zero in Cape Verde, agreeing with no significant horizontal velocity residuals relative to African-Nubian Plate motion in Cape Verde, becoming slightly higher towards the African coastline.

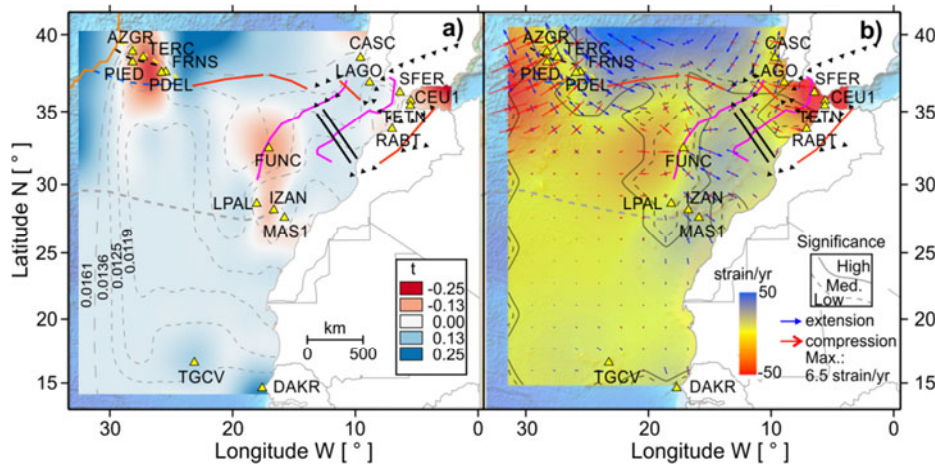


**Fig. 4.<sup>15</sup>** Macaronesia  $t$  parameter (Eq. (2)) and strain rate field maps for 2000–2015. **a)** Kinematic field based on  $t$  parameter rates;  $t$  prediction standard error rates shown with dotted and dashed isolines. **b)** Strain rate field represented by extension and compression. Inside two solid thin white lines<sup>16</sup>, the map shows a branch of low Curie point depth values that extends continuously from the Canary Archipelago to the Gulf of Cadiz, as in *Catalán et al. (2019)*. Black continuous, dashed and dotted curves delimit high, medium and low significance, respectively. See Fig. 1 for the meaning of individual features and Table 1 for GNSS station codes.<sup>17</sup>

1      Additionally, the strain was computed for the same grid. SSPX Software (*Cardozo and*  
 2      *Allmendinger, 2009*) and the grid strain package (*Teza et al., 2008*) were used to compute  
 3      the strain rate at the nodes of the grid. A total of 98 points with 17 real values in GNSS  
 4      stations (except FLRS and VILL) were included. For every grid node, the principal strain  
 5      rates (eigenvalues of the strain rate tensor) and the corresponding directions  
 6      (eigenvectors) were found. The grid resolution was set at 200 km and the grid distance  
 7      weighted routine was applied with a 300 km weighting factor to infer global patterns of  
 8      strain rates, where negative values indicate compression and positive values extension  
 9      (Fig. 4b). The strain rate allows distinction between regions with distinct tectonic  
 10     deformation patterns and boundaries between them as follows (Fig. 5):

- 11     • The Canary Islands archipelago presents horizontal residual velocities and a strain  
 12     rate similar to those of Madeira.  
 13     • North-eastward from the Canary Islands to southern Spain, on the Morocco  
 14     subplate, the strain rate has positive values (20 to 40 strain  $\text{yr}^{-1}$ ) with an azimuth of  
 15      $115^\circ$  (see also Fig. 4b), due to different velocity values between islands (lower)  
 16     and continents (higher).  
 17     • From westernmost Macaronesia towards the east, lower kinematic rates induced  
 18     a decrease in the extension rate, where the strain field changes from compression  
 19     of about 0 to  $-50$  strain  $\text{yr}^{-1}$  with an azimuth of  $60^\circ$  on the main axes to extension  
 20     of about 20 to 0 strain  $\text{yr}^{-1}$  with an azimuth of  $115^\circ$  near to the shear zone.

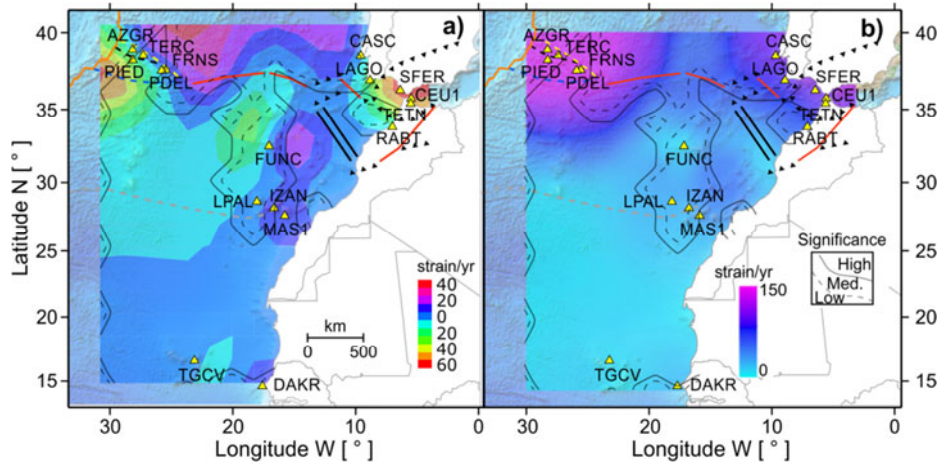


**Fig. 5.**<sup>18,19</sup> a) Macaronesia strain-rate changes for 2000–2015; b) rates of engineering shear normalised to strain-rate changes.<sup>20</sup>

- 1     • Extension rates close to 0 strain  $\text{yr}^{-1}$  appear to the east of the shear zone. Area
- 2       strain change and shear strain analysis showed a region from the Canary Islands
- 3       towards the Iberian Peninsula of 20 to 40 strain  $\text{yr}^{-1}$  (Fig. 5).
- 4     • The shear strain rate field further highlights the subdivision of Macaronesia into
- 5       four regions again: a) values of  $\sim 150$  strain  $\text{yr}^{-1}$  can be found in the north-west of
- 6       Macaronesia (Azores) with an extensional mechanism where the east of the Gloria
- 7       Fault is characterised by a dominant right-lateral strike-slip; b) the Strait of
- 8       Gibraltar is more diffuse with strain values of  $\sim 100$  strain  $\text{yr}^{-1}$ , a) and b) both
- 9       having high seismic activity and being located at plate boundaries (Fig. 1);
- 10      c) values of  $\sim 75$  strain  $\text{yr}^{-1}$  were obtained in the Canary Islands and Madeira
- 11      archipelago as intraplate strain; and d) values near zero were obtained for the Cape
- 12      Verde and Dakar regions (Fig. 5b).

## 13                   6. DISCUSSION

14     Three different approaches were used to analyse kinematics in the Macaronesia region,  
 15     from nearly 15-year-long time series, between 2000 and 2015, of 19 GNSS public  
 16     permanent stations. These GNSS time series are long enough to allow for horizontal  
 17     velocities with uncertainty of less than 1 mm  $\text{yr}^{-1}$  (*Blewitt and Lavallée, 2002*). The  
 18     horizontal velocities computed for the African-Nubian Plate show an average magnitude  
 19     of  $16.1 \pm 2.5$  mm  $\text{yr}^{-1}$  east and  $16.8 \pm 1.1$  mm  $\text{yr}^{-1}$  north with a mean module velocity of  
 20      $23.3 \pm 1.8$  mm  $\text{yr}^{-1}$  and direction of  $46.4^\circ \pm 5^\circ$ . The direction is comparable to that  
 21     obtained by NNR-MORVEL56 of  $44^\circ\text{N}$  in this zone (*Argus et al., 2011*) and similar to  
 22     those from previous GNSS studies (*Marques et al., 2013a; Miranda et al., 2012*). This

1 mean module velocity is analogous to the value in ITRF2008 using the UNAVCO Plate  
2 Motion Calculator that was applied as a standard value in the strain computation.

3 Rigidity seems to be a fundamental aspect of the African-Nubian Plate (*Burke and*  
4 *Wilson, 1972; Malservisi et al., 2013*) and recent kinematics from GNSS studies by  
5 *McClusky et al. (2003), Serpelloni et al. (2007)* and *Martín et al. (2014)* agree that there is  
6 no significant internal deformation ( $> 1 \text{ mm yr}^{-1}$ ). This new analysis shows values  
7  $> 1 \text{ mm yr}^{-1}$  using more stations, without episodic data and a longer observation interval  
8 than those previous studies. Only the horizontal velocity residual for Cape Verde (TGCV  
9 station), relative to NNR-MORVEL56, is under the GNSS precision ( $< 1 \text{ mm yr}^{-1}$ ), in  
10 agreement with global plate motion models, being the area where some authors locate the  
11 Euler pole for the African-Nubian Plate, therefore offering almost zero drift motion  
12 (*McClusky et al., 2003*). In all other areas, residuals are higher; for example, in Madeira  
13 and the Canary Islands, the horizontal residual velocities relative to the NNR-  
14 MORVEL56 model present values between 1 and 2  $\text{mm yr}^{-1}$ , and on the continental  
15 margin of Africa the values reach 2–3  $\text{mm yr}^{-1}$  (DAKR and RABT stations). As expected,  
16 stations in the Azores and Gibraltar arc regions present horizontal velocity residuals  
17 greater than 3  $\text{mm yr}^{-1}$ , influenced by their high seismicity, their proximity to plate  
18 boundaries and/or their location outside the African-Nubian Plate.

19 Different kinematic behaviours have been marked by the three different approaches  
20 applied. Firstly, the  $t$  parameter highlights anomalous kinematics in the oceanic intraplate  
21 (Canaries and Madeira archipelagos) and Azores archipelago as the main nonconforming  
22 velocity residuals (Fig. 4a).

23 Secondly, from cluster analysis, stations in the Azores archipelago were classified into  
24 three different groups. Although PDEL and FRNS stations are both on São Miguel Island,  
25 they were assigned to African-Nubian and Eurasian groups, respectively. Furthermore,  
26 FRNS not only has different horizontal ground displacement compared to PDEL but also  
27 has twice the subsidence of PDEL. This separation within São Miguel has already been  
28 identified previously (*DeMets et al., 1994; Marques et al., 2013a; Weiss et al., 2015*), here  
29 with an inferred extension strain rate of near 13 strain/yr and azimuth of 260°. AZGR and  
30 TER, with a strain rate of near 6 strain  $\text{yr}^{-1}$  and azimuth of 253°, were not assigned to  
31 either the Eurasian or Nubian–Macaronesian Islands groups. This is due to the influence  
32 of the Terceira Rift extension and is in agreement with previous studies (*Marques et al.,*  
33 *2015; Mendes et al., 2013; Miranda et al., 2012*). PIED on Pico island and PDEL were  
34 grouped with Madeira, Canary Islands and Cape Verde stations, therefore with Nubian-  
35 Macaronesian behaviour, however revealing ground displacement slightly induced by the  
36 Terceira Rift (*Hipólito et al., 2014; Madeira et al., 2015*). Although cluster analysis  
37 detected differences on São Miguel, it did not detect significant differences on the Canary  
38 Islands, despite the clear azimuth difference of the velocity residuals of IZAN station in  
39 Tenerife. Nevertheless, within the Canary Islands, compression was inferred west and  
40 extension was inferred east, following previous studies. In the numerical stress model  
41 from *Geyer et al. (2016)*, areas of deformation were deduced from local structural  
42 discontinuities which depend on pressure values applied to the EAFZ. The strain rate in  
43 the Canary Islands was calculated as positive (extension) in the NW-SE direction. This  
44 direction is perpendicular to the NE-SW line that coincides with a seismically active  
45 oblique reverse fault that separates the Tenerife (NE orientation) and Gran Canaria (SE

1 orientation) insular blocks (*Ruiz et al., 2000*), with a transpression regime area with  
2 a strain rate of 17 strain  $\text{yr}^{-1}$ .

3 Strain rate computation also showed, between Madeira and the continental margin of  
4 Africa, an inferred WNW-ESE to NE-SW change in orientation of the main extensional  
5 strain that may be explained by a high seismicity transform fault proposed by *Mantovani*  
6 *et al.* (2007) (delimited by two thick black solid curves). There is an NE-SW extensional  
7 strain rate and higher change area rates which progress from the north-western part of the  
8 Canary Archipelago to the Gulf of Cadiz, which coincide with the shallowest Curie point  
9 depths. These values were obtained in oceanic domains, being constant along this track,  
10 supporting the presence of an nospheric connection between both locations (*Catalán et*  
11 *al., 2019*) or an active mantle upwelling from a remnant plume (*Miller et al., 2015; Saki et*  
12 *al., 2015*). The higher horizontal velocity for the stations on the continental margin of  
13 Africa compared to those of Madeira, the Canary Islands and Cape Verde, although nearly  
14 perpendicular, promotes a slight compression north of the Canary Islands and extension  
15 south, near the continental margin. In the Gibraltar arc, the SFER velocity residual has  
16 greater similarity to those of the North-African GNSS stations (CEU1 or TETN),  
17 compared to CASC and LAGO also on the Iberian Peninsula. The azimuths in this region  
18 indicate a rotation to accommodate a Gibraltar arc slow subduction rate and possible slab  
19 roll-back, which may be responsible for the arc propagation towards Atlantic domains  
20 (*Duarte et al. 2013; Vernant et al., 2010*). Furthermore, the inferred NW-SE compression  
21 south-west of the Iberian Peninsula and W-E west of Gibraltar are both compatible with  
22 corresponding geological structures - the Gorringe ridge and the Gibraltar arc,  
23 respectively (*Duarte et al., 2013; Zitellini et al., 2009*). The Gibraltar arc region presents  
24 high seismic activity, overlapping faults (*Geyer et al., 2016; Jiménez-Munt and Negredo,*  
25 *2003; Negredo et al., 2002*) and a widespread transition between plates already shown by  
26 several GNSS studies (*de Lis Mancilla et al., 2013; Koulali et al., 2011; López et al.,*  
27 *2017; Zitellini et al., 2009*). Our results are consistent with these structures defined by all  
28 these previous studies.

29 Regarding the height component, there is an overall subsidence, except for at the  
30 DAKR and TGCV stations. All oceanic stations show this trend over 15 years. This  
31 negative trend is similar to those from other recent GNSS studies (*López et al., 2017;*  
32 *Miranda et al., 2012*) and DInSAR results. Top values are located in the Terceira Rift  
33 group in the Azores (TERC nearly  $-9 \text{ mm yr}^{-1}$  and AZGR  $-5 \text{ mm yr}^{-1}$ ) and, without  
34 ruling out possible local effects, this behaviour could be related to down-bending of the  
35 crust by the weight of material added to the crust by active volcanoes, similar to the  
36 isostatic adjustment of Miocene islands (*Moore, 1970*). The subsidence in Madeira and  
37 the Canary Islands could be also explained by a partial magma withdrawal at different  
38 depths in the mantle (*Klügel et al., 2015*).

## 39 7. CONCLUSIONS

40 This study approximates present day relative motion in Macaronesia, a geographical  
41 area in the north-east Atlantic ocean, based on GNSS data from 19 permanent stations  
42 with a long observation period of nearly 15 years (from May 2000 to March 2015).  
43 Although previous GNSS studies found no intraplate deformation, this analysis found

1 velocity residuals in regions with low to non-existent seismic activity, specifically: greater  
2 than 1 mm yr<sup>-1</sup> in Madeira, between 1 and 2 mm yr<sup>-1</sup> in the Canary Islands and between  
3 2 and 3 mm yr<sup>-1</sup> on the continental margin of Africa (DAKR and RABT stations). In  
4 addition, stations in the Azores and Gibraltar arc regions present horizontal velocity  
5 residuals greater than 3 mm yr<sup>-1</sup>, influenced mainly by their proximity to plate boundaries  
6 and with directions according to previous studies.

7 The similar kinematic behaviour between islands is not followed by stations on the  
8 continental margin of Africa. The difference in magnitude, but particularly in azimuth,  
9 causes the inferred strain rate extension NW-SE in the Canary Islands to shift to W-E to  
10 the east of Madeira and NE-SW at the Gloria Fault. From seismicity, kinematic and strain  
11 data analysis, a shear zone was located in harmony with other studies (*Mantovani et al.*,  
12 2007). Seismic activity and strain rates suggest some dextral strike-slip deformation  
13 occurring within the Morocco subplate along a NNW-SSE direction from the Gorringe  
14 Bank to Agadir, and/or a remnant mantel plume upwelling (*Saki et al.*, 2015).

15 In the Canary archipelago, horizontal residual velocities show a slight azimuth shift  
16 that affects the strain rate between Tenerife and Gran Canaria. The strain rate in the  
17 Canary Islands, inferred as positive (extension) in the NW-SE direction, is perpendicular  
18 to the NE-SW seismically active oblique reverse fault identified in previous studies  
19 (*Barbero et al.*, 2018). It could be also due to a temporary magma accumulation zone that  
20 contributes to deep endogenous growth and uplift of the volcanoes.

21 All GNSS stations in the Macaronesian islands show subsidence, possibly linked to  
22 isostatic adjustment of volcanic islands (*Moore*, 1970). Finally, although this study  
23 presents large areas without GNSS stations, limiting conclusions there, in regions covered  
24 by several GNSS stations our GNSS data analysis presents consistency with and support  
25 to previous local studies, providing an overall interpretation of the recent intraplate  
26 kinematics of the African-Nubian Plate, particularly between emerged land.

27

28

#### 29 *References<sup>21</sup>*

- 30 Argus D.F., Gordon R.G. and Demets C., 2011. Geologically current motion of 56 plates relative to  
31 the no-net-rotation reference frame. *Geochem. Geophys. Geosyst.*, **12**, Art.No. Q11001,  
32 DOI: 10.1029/2011GC003751
- 33 Barbero I., Torrecillas C., Prates G., Páez R., Gárate J., García A. and Berrocoso M., 2018.  
34 Assessment of ground deformation following Tenerife's 2004 volcanic unrest (Canary  
35 Islands). *J. Geodyn.*, **121**, 1–8, DOI: 10.1016/j.jog.2018.06.002
- 36 Blewitt G. and Lavallée D., 2002. Effect of annual signals on geodetic velocity. *J. Geophys. Res.-*  
37 *Solid Earth*, **107**, Art.No. 2145, DOI: 10.1029/2001JB000570
- 38 Borges J.F.F., Bezzeghou M., Buforn E., Pro C. and Fitas A., 2007. The 1980, 1997 and 1998  
39 Azores earthquakes and some seismo-tectonic implications. *Tectonophysics*, **435**, 37–54,  
40 DOI: 10.1016/j.tecto.2007.01.008
- 41 Bos M.S., Bastos L. and Fernandes R.M.S., 2010. The influence of seasonal signals on the  
42 estimation of the tectonic motion in short continuous GPS time-series. *J. Geodyn.*, **49**,  
43 205–209, DOI: 10.1016/j.jog.2009.10.005

- 1 Bos M.S., Fernandes R.M.S., Williams S.D.P. and Bastos L., 2013. Fast error analysis of continuous  
2 GNSS observations with missing data. *J. Geodesy*, **87**, 351–360, DOI: 10.1007/s00190-012-  
3 0605-0
- 4 Burke K. and Wilson J.T., 1972. Is the African Plate stationary? *Nature*, **239**, 387–390,  
5 DOI: 10.1038/239387b0
- 6 Calais E., DeMets C. and Nocquet J.M., 2003. Evidence for a post-3.16-Ma change in Nubian-  
7 Eurasia-North America plate motions? *Earth Planet. Sci. Lett.*, **216**, 81–92, DOI: 10.1016/  
8 /S0012-821X(03)00482-5
- 9 Cardozo N. and Allmendinger R.W., 2009. SSPX: A program to compute strain from  
10 displacement/velocity data. *Comput. Geosci.*, **35**, 1343–1357, DOI: 10.1016/  
11 /j.cageo.2008.05.008
- 12 Catalán M., Martos Y.M. and Martín-Davila J., 2019. Eurasia-Africa plate boundary affected by  
13 a South Atlantic asthenospheric channel in the Gulf of Cadiz region? *Pure Appl. Geophys.*,  
14 **177**, 1725–1738, DOI: 10.1007/s00024-019-02380-4
- 15 Dach R., Hugentobler U. and Walser P., 2011. *Tutorial Processing Example Introductory Course*  
16 *Terminal Session*. <http://www.bernese.unibe.ch/docs50/TERMINAL.pdf>
- 17 de Lis Mancilla F., Stich D., Berrocoso M., Martín R., Morales J., Fernandez-Ros A., Páez R., and  
18 Perez-Pena A., 2013. Delamination in the Betic Range: Deep structure, seismicity, and GPS  
19 motion. *Geology*, **41**, 307–310, DOI: 10.1130/G33733.1
- 20 DeMets C., Gordon R.G. and Argus D.F., 2010. Geologically current plate motions. *Geophys. J. Int.*,  
21 **181**, 1–80, DOI: 10.1111/j.1365-246X.2009.04491.x
- 22 DeMets C., Gordon R.G., Argus D.F. and Stein S., 1994. Effect of recent revisions to the  
23 geomagnetic resersal time-scale on estimates of current plate motions. *Geophys. Res. Lett.*, **21**,  
24 2191–2194, DOI: 10.1029/94GL02118
- 25 Dias P., Catalao J. and Marques F.O., 2018. Sentinel-1 InSAR data applied to surface deformation  
26 in Macaronesia (Canaries and Cape Verde). *Procedia Computer Science*, **138**, 382–387,  
27 DOI: 10.1016/j.procs.2018.10.054
- 28 Domínguez-Cerdeña I., del Fresno C. and Rivera L., 2011. New insight on the increasing seismicity  
29 during Tenerife's 2004 volcanic reactivation. *J. Volcanol. Geotherm. Res.*, **206**, 15–29,  
30 DOI: 10.1016/j.jvolgeores.2011.06.005
- 31 Duarte J.C., Rosas F.M., Terrinha P., Schellart W.P., Boutelier D., Gutscher M.A. and Ribeiro A.,  
32 2013. Are subduction zones invading the atlantic? Evidence from the southwest iberia margin.  
33 *Geology*, **41**, 839–842, DOI: 10.1130/G34100.1
- 34 Fernandes R.M.S., Bastos L., Miranda J.M., Lourenço N., Ambrosius B.A.C., Noomen R. and  
35 Simons W., 2006. Defining the plate boundaries in the Azores region. *J. Volcanol. Geotherm.*  
36 *Res.*, **156**, 1–9, DOI: 10.1016/j.jvolgeores.2006.03.019
- 37 Garcia A., Fernandez-Ros A., Berrocoso M., Marrero J.M., Prates G., De la Cruz-Reyna S. and  
38 Ortiz R., 2014. Magma displacements under insular volcanic fields, applications to eruption  
39 forecasting: El Hierro, Canary Islands, 2011–2013. *Geophys. J. Int.*, **197**, 322–334,  
40 DOI: 10.1093/gji/ggt505
- 41 Geldmacher J., Hoernle K., Klügel A., von den Bogaard P., Wombacher F. and Berning B., 2006.  
42 Origin and geochemical evolution of the Madeira-Tore Rise (eastern North Atlantic).  
43 *J. Geophys. Res.-Solid Earth*, **111**, Art.No. B09206, DOI: 10.1029/2005JB003931

- 1 Geldmacher J., Hoernle K., Klügel A., von den Bogaard P. and Duggen S., 2006. A geochemical  
2 transect across a heterogeneous mantle upwelling: Implications for the evolution of the  
3 Madeira hotspot in space and time. *Lithos*, **90**, 131–144, DOI: 10.1016/j.lithos.2006.02.004
- 4 Geyer A., Martí J. and Villaseñor A., 2016. First-order estimate of the Canary Islands plate-scale  
5 stress field: Implications for volcanic hazard assessment. *Tectonophysics*, **679**, 125–139,  
6 DOI: 10.1016/j.tecto.2016.04.010
- 7 Goudarzi M.A., Cocard M. and Santerre R., 2014. EPC: Matlab software to estimate Euler pole  
8 parameters. *GPS Solut.*, **18**, 153–162, DOI: 10.1007/s10291-013-0354-4
- 9 He X., Montillet J.P., Hua X., Yu K., Jiang W. and Zhou F., 2017. Noise analysis for environmental  
10 loading effect on GPS position time series. *Acta Geodyn. Geomater.*, **14**, 131–142,  
11 DOI: 10.13168/AGG.2016.0034
- 12 Heidbach O., Rajabi M., Cui X., Fuchs K., Müller B., Reinecker J., Reiter K., Tingay M., Wenzel  
13 F., Xie F.R., Ziegler M.O. and Zoback M.L., 2018. The World Stress Map database release  
14 2016: Crustal stress pattern across scales. *Tectonophysics*, **744**, 484–498, DOI: 10.1016  
15 /j.tecto.2018.07.007
- 16 Hipólito A., Hipólito A., Madeira J., Carmo R. and Gaspar J.L., 2014. Neotectonics of Graciosa  
17 island (Azores): a contribution to seismic hazard assessment of a volcanic area in a complex  
18 geodynamic setting. *Ann. Geophys.*, **56**, Art.No. S0677, DOI: 10.4401/ag-6222
- 19 International Seismological Centre, 2019. *On-line Bulletin*, DOI: 10.31905/D808B830  
20 (<http://www.isc.ac.uk/iscbulletin/>)
- 21 Jiménez-Munt I. and Negredo A.M., 2003. Neotectonic modelling of the western part of the Africa-  
22 Eurasia plate boundary: from the Mid-Atlantic ridge to Algeria. *Earth Planet. Sci. Lett.*, **205**,  
23 257–271, DOI: 10.1016/S0012-821X(02)01045-2
- 24 Kaufman L. and Rousseeuw P.J., 1990. *Finding Groups in Data*. John Wiley and Sons, Hoboken,  
25 NJ, DOI: 10.1002/9780470316801
- 26 Klos A., Bos M.S. and Bogusz J., 2018. Detecting time-varying seasonal signal in GPS position  
27 time series with different noise levels. *GPS Solut.*, **22**, Art.No. UNSP21,  
28 DOI: 10.1007/s10291-017-0686-6
- 29 Klos A., Bos M.S., Fernandes R.M.S. and Bogusz J., 2019. Noise-dependent adaption of the Wiener  
30 filter for the GPS position time series. *Math. Geosci.*, **51**, 53–73, DOI: 10.1007/s11004-018-  
31 9760-z
- 32 Klügel A., Longpré M.A., García-Cañada L. and Stix J., 2015. Deep intrusions, lateral magma  
33 transport and related uplift at ocean island volcanoes. *Earth Planet. Sci. Lett.*, **431**, 140–149,  
34 DOI: 10.1016/j.epsl.2015.09.031
- 35 Kogan M.G., Steblov G.M., King R.W., Herring T.A., Frolov D.I., Egorov S.G., Levin V.Y.,  
36 Lerner-Lam A. and Jones A., 2000. Geodetic constraints on the rigidity and relative motion of  
37 Eurasia and North America. *Geophys. Res. Lett.*, **27**, 2041–2044, DOI: 10.1029  
38 /2000GL011422
- 39 Koulali A., Ouazar D., Tahayt A., King R.W., Vernant P., Reilinger R.E., McClusky S.,  
40 Mourabit T., Davila J.M. and Amraoui N., 2011. New GPS constraints on active deformation  
41 along the Africa-Iberia plate boundary. *Earth Planet. Sci. Lett.*, **308**, 211–217, DOI: 10.1016  
42 /j.epsl.2011.05.048
- 43 Larose D.T. and Larose C.D., 2014. Hierarchical and k-means clustering. *Discovering Knowledge in  
44 Data*, 209–227, John Wiley and Sons, Hoboken, NJ, DOI: 10.1002/9781118874059.ch10

- 1 López C., García-Cañada L., Martí J. and Domínguez Cerdeña I., 2017. Early signs of geodynamic  
2 activity before the 2011–2012 El Hierro eruption. *J. Geodyn.*, **104**, 1–14, DOI: 10.1016/j.jog.2016.12.005
- 3
- 4 Madeira J., Brum da Silveira A., Hipólito A. and Carmo R., 2015. Chapter 3 Active tectonics in the  
5 central and eastern Azores islands along the Eurasia-Nubian boundary: a review. *Geol. Soc.  
6 London Mem.*, **44**, 15–32, DOI: 10.1144/m44.3
- 7 Malservisi R., Hugentobler U., Wonnacott R. and Hackl M., 2013. How rigid is a rigid plate?  
8 Geodetic constraint from the TrigNet CGPS network, South Africa. *Geophys. J. Int.*, **192**,  
9 918–928, DOI: 10.1093/gji/ggs081
- 10 Mantovani E., Viti M., Babbucci D. and Albarello D., 2007. Nubian-Eurasia kinematics: An  
11 alternative interpretation from Mediterranean and North Atlantic evidence. *Ann. Geophys.*, **50**,  
12 341–366, DOI: 10.4401/ag-3073
- 13 Marques F.O., Catalão J., Hildenbrand A. and Madureira P., 2015. Ground motion and tectonics in  
14 the Terceira Island: Tectonomagmatic interactions in an oceanic rift (Terceira Rift, Azores  
15 Triple Junction). *Tectonophysics*, **651**, 19–34, DOI: 10.1016/j.tecto.2015.02.026
- 16 Marques F.O., Catalão J.C., DeMets C., Costa A.C.G. and Hildenbrand A., 2013. GPS and tectonic  
17 evidence for a diffuse plate boundary at the Azores Triple Junction. *Earth Planet. Sci. Lett.*,  
18 **381**, 177–187, Elsevier B.V, DOI: 10.1016/j.epsl.2013.08.051
- 19 Martín A., Sevilla M. and Zurutuza J., 2014. Crustal deformation study in the Canary Archipelago  
20 by the analysis of GPS observations. *J. Appl. Geodesy*, **8**, 129–140, DOI: 10.1515/jag-2014-  
21 0002
- 22 McClusky S., Reilinger R., Mahmoud S., Ben Sari D. and Tealeb A., 2003. GPS constraints on  
23 Africa (Nubian) and Arabia plate motions. *Geophys. J. Int.*, **155**, 126–138, DOI: 10.1046  
24 /j.1365-246X.2003.02023.x
- 25 Mendes V.B., Madeira J., Brum da Silveira A., Trota A., Elosegui P. and Pagarete J., 2013. Present-  
26 day deformation in São Jorge Island, Azores, from episodic GPS measurements (2001–2011).  
27 *Adv. Space Res.*, **51**, 1581–1592, DOI: 10.1016/j.asr.2012.10.019
- 28 Mervart L., 1995. *Ambiguity Resolution Techniques in Geodetic and Geodynamic Applications of  
29 the Global Positioning System*. PhD Thesis. University of Bern, Bern, Switzerland.
- 30 Métrich N., Zanon V., Créon L., Hildenbrand A., Moreira M. and Marques F.O., 2014. Is the  
31 ‘Azores Hotspot’ a wetspot? Insights from the geochemistry of fluid and melt inclusions in  
32 olivine of Pico basalts. *J. Petrol.*, **55**, 377–393, DOI: 10.1093/petrology/egt071
- 33 Miller M.S., O'Driscoll L.J., Butcher A.J. and Thomas C., 2015. Imaging Canary Island hotspot  
34 material beneath the lithosphere of Morocco and southern Spain. *Earth Planet. Sci. Lett.*, **431**,  
35 186–194, DOI: 10.1016/j.epsl.2015.09.026
- 36 Miranda J.M., Navarro A., Catalão J. and Fernandes R.M.S., 2012. Surface displacement field at  
37 Terceira island deduced from repeated GPS measurements. *J. Volcanol. Geotherm. Res.*,  
38 **217–218**, 1–7, DOI: 10.1016/j.volgeores.2011.10.009
- 39 Moore J.G., 1970. Relationship between subsidence and volcanic load, Hawaii. *Bull. Volcanol.*, **34**,  
40 562–576, DOI: 10.1007/BF02596771
- 41 Negredo A.M., Bird P., Sanz de Galdeano C. and Buorn E., 2002. Neotectonic modeling of the  
42 Ibero-Maghrebian region. *J. Geophys. Res.-Solid Earth*, **107**, Art.No. 2292,  
43 DOI: 10.1029/2001JB000743

- 1 Niell A.E., 2004. Global mapping functions for the atmosphere delay at radio wavelengths.  
2 *J. Geophys. Res.-Solid Earth*, **101**, 3227–3246, DOI: 10.1029/95jb03048
- 3 Özdemir S. and Karşioğlu M.O., 2019. Soft clustering of GPS velocities from a homogeneous  
4 permanent network in Turkey. *J. Geodesy*, **93**, 1171–1195, DOI: 10.1007/s00190-019  
5 -01235-z
- 6 Pacheco J.M., Ferreira T., Queiroz G., Wallenstein N., Coutinho R., Cruz J.V., Pimentel A.,  
7 Silva R., Gaspar J.L. and Goulart C., 2013. Notas sobre a geologia do arquipélago dos Açores.  
8 In: Dias R., Araújo A., Terrinha P. and Kullberg J.C. (Eds), *Geologia de Portugal*. Vol. 2,  
9 595–690, Escolar Editora, Lisbon, Portugal (in Portuguese).
- 10 Pérez-Peña A., Martín-Davila J., Gárate J., Berrocoso M. and Buforn E., 2010. Velocity field and  
11 tectonic strain in Southern Spain and surrounding areas derived from GPS episodic  
12 measurements. *J. Geodyn.*, **49**, 232–240, DOI: 10.1016/j.jog.2010.01.015
- 13 Prates G., García A., Fernández-Ros A., Marrero J.M., Ortiz R. and Berrocoso M., 2013.  
14 Enhancement of sub-daily positioning solutions for surface deformation surveillance at El  
15 Hierro volcano (Canary Islands, Spain). *Bull. Volcanol.*, **75**, Art.No. 724, DOI: 10.1007  
16 /s00445-013-0724-3
- 17 Ramalho R.A.S., 2011. The Cape Verde Archipelago. *Building the Cape Verde Islands*, Springer-  
18 Verlag, Berlin, Germany, 13–26, DOI: 10.1007/978-3-642-19103-9\_2
- 19 Ray R.D., 1999. *A Global Ocean Tide Model From TOPEX/POSEIDON Altimetry: GOT99.2*.  
20 Technical Memorandum 1999-209478. NASA Goddard Space Flight Center, Greenbelt, MD
- 21 Rebischung P., Altamimi Z., Ray J. and Garayt B., 2016. The IGS contribution to ITRF2014.  
22 *J. Geodesy*, **90**, 611–630, DOI: 10.1007/s00190-016-0897-6
- 23 Rousseeuw P.J., 1987. Silhouettes: A graphical aid to the interpretation and validation of cluster  
24 analysis. *J. Comput. Appl. Math.*, **20**, 53–65, DOI: 10.1016/0377-0427(87)90125-7
- 25 Ruiz C.R., García-Cacho L., Araña V., Luque A.Y. and Felpeto A., 2000. Submarine volcanism  
26 surrounding Tenerife, Canary Islands: Implications for tectonic controls, and oceanic shield  
27 formingprocesses. *J. Volcanol. Geotherm. Res.*, **103**, 105–119, DOI: 10.1016/S0377-0273  
28 (00)00218-3
- 29 Saastamoinen J., 2013. Atmospheric correction for the troposphere and stratosphere in radio ranging  
30 satellites. In: Henriksen S.W., Mancini A. and Chovitz B.H. (Eds), *The Use of Artificial  
31 Satellites for Geodesy*, Volume 15. American Geophysical Union, Washington, D.C.,  
32 247–251, DOI: 10.1029/GM015p0247
- 33 Saki M., Thomas C., Nippes S.E.J. and Lessing S., 2015. Topography of upper mantle seismic  
34 discontinuities beneath the North Atlantic: The Azores, Canary and Cape Verde plumes. *Earth  
35 Planet. Sci. Lett.*, **409**, 193–202, DOI: 10.1016/j.epsl.2014.10.052
- 36 Savage J.C. and Simpson R.W., 2013. Clustering of GPS velocities in the Mojave Block,  
37 southeastern California. *J. Geophys. Res.-Solid Earth*, **118**, 1747–1759, DOI: 10.1029  
38 /2012JB009699
- 39 Scheidegger A.E., 2002. Morphometric analysis and its relation to tectonics in Macaronesia.  
40 *Geomorphology*, **46**, 95–115, DOI: 10.1016/S0169-555X(02)00056-9
- 41 Scherneck H.-G. and Bos M.S., 2002. Ocean tide and atmospheric loading. In: Vandenberg N.R.  
42 and Baver K.D. (Eds), *IVS 2002 General Meeting Proceedings*. NASA/CP-2012-217504,  
43 NASA Goddard Space Flight Center, Greenbelt, MD, 205–214.  
44 [http://publications.lib.chalmers.se/records/fulltext/local\\_158760.pdf](http://publications.lib.chalmers.se/records/fulltext/local_158760.pdf)

- 1 Serpelloni E., Vannucci G., Pondrelli S., Argnani A., Casula G., Anzidei M., Baldi P. and Gasperini  
2 P., 2007. Kinematics of the Western Africa-Eurasia plate boundary from focal mechanisms  
3 and GPS data. *Geophys. J. Int.*, **169**, 1180–1200, DOI: 10.1111/j.1365-246X.2007.03367.x
- 4 Silva P.F., Henry B., Marques F.O., Hildenbrand A., Lopes A., Madureira P., Madeira J., Nunes J.C.  
5 and Roxerova Z., 2018. Volcano-tectonic evolution of a linear volcanic ridge (Pico-Faial  
6 Ridge, Azores Triple Junction) assessed by paleomagnetic studies. *J. Volcanol. Geotherm.  
7 Res.*, **352**, 78–91, Elsevier B.V, DOI: 10.1016/j.jvolgeores.2018.01.005
- 8 Silveira G., Vinnik L., Stutzmann E., Farra V., Kiselev S. and Morais I., 2010. Stratification of the  
9 Earth beneath the Azores from P and S receiver functions. *Earth Planet. Sci. Lett.*, **299**,  
10 91–103, DOI: 10.1016/j.epsl.2010.08.021
- 11 Simpson R.W., Thatcher W. and Savage J.C., 2012. Using cluster analysis to organize and explore  
12 regional GPS velocities. *Geophys. Res. Lett.*, **39**, Art.No. L18307, DOI: 10.1029/  
13 /2012GL052755
- 14 Teza G., Pesci A. and Casula G., 2012. Strain rate computation in Northern Victoria Land  
15 (Antarctica) from episodic GPS surveys. *Geophys. J. Int.*, **189**, 851–862, DOI: 10.1111/  
16 /j.1365-246X.2012.05403.x
- 17 Teza G., Pesci A. and Galgaro A., 2008. Grid\_strain and grid\_strain3: Software packages for strain  
18 field computation in 2D and 3D environments. *Comput. Geosci.*, **34**, 1142–1153,  
19 DOI: 10.1016/j.cageo.2007.07.006
- 20 von den Bogaard P., 2013. The origin of the Canary Island Seamount Province - New ages of old  
21 seamounts. *Sci. Rep.*, **3**, Art.No. 2107, DOI: 10.1038/srep02107
- 22 Vernant P., Fadil A., Mourabit T., Ouazar D., Koulali A., Davila J.M., Garate J., McClusky S. and  
23 Reilinger R., 2010. Geodetic constraints on active tectonics of the Western Mediterranean:  
24 Implications for the kinematics and dynamics of the Nubian-Eurasia plate boundary zone.  
25 *J. Geodyn.*, **49**, 123–129, DOI: 10.1016/j.jog.2009.10.007
- 26 Weiss B.J., Hübscher C. and Lüdmann T., 2015. The tectonic evolution of the southeastern Terceira  
27 Rift/São Miguel region (Azores). *Tectonophysics*, **654**, 75–95, DOI: 10.1016/j.tecto.2015.04.018
- 28 Williams S.D.P., Bock Y., Fang P., Jamason P., Nikolaidis R.M., Prawirodirdjo L., Miller M. and  
29 Johnson D.J., 2004. Error analysis of continuous GPS position time series. *J. Geophys. Res.-  
30 Solid Earth*, **109**, Art.No. B03412, DOI: 10.1029/2003jb002741
- 31 Zitellini N., Grácia E., Matias L., Terrinha P., Abreu M.A., DeAlterriis G., Henriet J.P.,  
32 Danobeitia J.J., Masson D.G., Mulder T., Ramella R., Somoza L. and Diez S., 2009. The quest  
33 for the Africa-Eurasia plate boundary west of the Strait of Gibraltar. *Earth Planet. Sci. Lett.*,  
34 **280**, 13–50, DOI: 10.1016/j.epsl.2008.12.005
- 35
- 36
- 37
- 38

---

<sup>1</sup> Please, specify also the city.

<sup>2</sup> Please, check and approve the edit.

<sup>3</sup> Please, check and approve the edit.

<sup>4</sup> Please, check and approve the edit and define GB.

<sup>5</sup> Please, check and approve the edit.

<sup>6</sup> Do you mean country, or subplate?

<sup>7</sup> Please, check and approve the edit.

<sup>8</sup> Please, check and approve the edit.

<sup>9</sup> Please, approve formatting of the parameters.

<sup>10</sup> This seems to be missing in the table.

<sup>11</sup> Please, check and approve the edit.

<sup>12</sup> Please, define these parameters (standard deviations?)

<sup>13</sup> Please, check and approve the edit.

<sup>14</sup> Please, check and approve the edit.

<sup>15</sup> In the bw version of this figure, please, modify the part a). The bw scale has the same greys for different values. Change it from light do dark.

<sup>16</sup> These are not visible.

<sup>17</sup> Please, check and approve the edit.

<sup>18</sup> The colored scale in a) is unclear, the same values are used for different colors. Please, clarify.

<sup>19</sup> The same as in the bw case of Fig. 4a. Moreover, in bw Fig. 5b the scale does not correspond to the plot, there are darker greys in the plot.

<sup>20</sup> Please, check and approve the edit.

<sup>21</sup> References were formatted according to our style. Please, check them all carefully. Make also sure that all the references are cited in the text (and vice versa, all the references cited in the text are listed in the list of references).